Thermoelectrochemistry using conventional and novel gelled electrolytes in heat-to-current thermocells

Jimmy Wu,[a] *Jeffrey J. Black,*[a] *and Leigh Aldous*[a]*

[a] School of Chemistry, UNSW Australia, Sydney, NSW 2052, Australia

* l.aldous@unsw.edu.au

To be published in ***Electrochimica Acta***

Publishers' version can be found at
http://dx.doi.org/10.1016/j.electacta.2016.12.152

Accepted by publisher: **24th December 2016**
Made available online by publisher: **26th December 2016**
Uploaded to kclpure by authors: **16th February 2017**
Embargoed on kclpure until: **26th December 2017**

ABSTRACT

Thermoelectrochemistry involves the study or application of temperature-dependant parameters in an electrochemical system. Thermoelectrochemistry can be exploited in non-isothermal cells to form thermogalvanic cells (or thermocells) to convert a temperature gradient into a useful electrical current. However, heat can also transfer and reduce the temperature gradient, while spillage is a potential issue for liquid electrolytes. For this reason, we have investigated aqueous thermocells containing potassium ferricyanide and potassium ferrocyanide (0.1 M $K_3[Fe(CN)_6]$ / 0.1 M $K_4[Fe(CN)_6]$) as a gelled electrolyte. Fumed silica and gelatine were not found to be sufficient gelling agents, whereas agar agar (agarose) and beads of poly(sodium acrylate) were found to form effective gelled electrolytes; the latter gel was also self-healing. Thermocells were prepared using commercial CR2032 battery casings, and surface treatments and preparations of the stainless steel electrodes evaluated for their electrocatalytic effects and influence on long-term current output. Emphasis was placed upon body heat harvesting, and preliminary heat transfer modelling through the CR2032 systems also performed. Ultimately, the gelled electrolytes were found to result in more stable power output and effectively frustrate heat transfer through the cells, relative to the un-gelled (liquid) electrolytes. These results will inform the development of both more efficient electrolytes and housings for thermocells.

Keywords: gelled electrolyte; thermocell; electrocatalysis; stainless steel; thermoelectrochemical; waste thermal energy

1. Introduction

Electrochemistry has revolutionised modern lifestyles and quality of life, particularly in the areas of energy storage and conversion. Thermoelectrochemistry offers a relatively elegant method for the (electrochemical) conversion of a temperature difference into an electrical current.[1, 2] It relies upon an entropy difference between the two sides of a redox process; therefore a potential difference (ΔE) can be generated across two electrodes that are directly proportional to the temperature difference between two electrodes (ΔT) and the overall or total entropy change resulting from the redox process. The resulting temperature-dependant potential difference is typically summarised as the Seebeck coefficient, S_e, as shown by equation (1). The entropy changes relate to at least the entropy change due to the electrode reaction, the various entropies of transfer, and the transported entropy of the electrons, as discussed extensively elsewhere.[2-5] The observed potential is also subject to other non-equilibrium effects, such as the Soret effect.[2, 5, 6]

$$S_e = \frac{\Delta E}{\Delta T} \tag{1}$$

In its simplest incarnation, thermoelectrochemistry is based upon a temperature difference between two electrodes sharing a common redox-active electrode.[3] Thus an electrical current stems from a temperature-driven redox process, and thermoelectrochemistry is therefore somewhat analogous to thermoelectric devices where a temperature difference across a semiconductor drives electron or hole transport through said semiconductor.[7] The efficiency of both devices is limited by the maximum possible Carnot efficiency.[2]

Thermoelectrics are typically based on solid-state, rare-earth semiconductors which are incompatible with exposure to repeated temperature gradients and have Seebeck coefficients on the order of μV K^{-1}.[8] They are therefore reserved for niche applications, typically under extreme

conditions, such as space exploration.[8] Conversely, thermoelectrochemical systems can be based on exclusively solid[9], liquid[1] or molten[2] electrolytes, or any combination of solid, liquid and even gaseous[10] electrodes and electrolytes. Significantly higher Seebeck coefficients, on the order of mV K^{-1}, are taken as standard.[1, 2] As the efficiency of heat-to-current conversion is directly proportional to both the temperature difference and the Seebeck coefficient squared, the exceptional Seebeck coefficients of thermoelectrochemical systems have encouraged their investigation for efficient thermal energy harvesting of low-grade sources, such as body heat.[11-13] Nanostructuring the electrodes has also been demonstrated to be relatively facile but highly beneficial.[14, 15]

The high Seebeck coefficients common to effective thermoelectrochemical systems are typically driven by significant changes in the aqueous solvation sphere around ions.[14] Aqueous solutions of ferricyanide and ferrocyanide are commonly employed as a *pseudo*-standard, by virtue of the redox system's respectable Seebeck coefficient (*ca.* -1.4 mV K^{-1})[7] and relatively fast electron transfer constants (under ideal conditions).[16] However, a vast range of possible interactions (which have barely begun to be investigated) are also possible entropic driving forces, *e.g.* explicitly coordinating non-aqueous media,[14] high spin low spin transitions,[17] electrode side reactions,[11] electrode intercalation processes[18] and solution-phase synergistic interactions.[19]

Liquid electrolytes are effective for thermoelectrochemical systems (or 'thermocells'), insomuch as they can possess high Seebeck coefficients for certain redox couples, typically possess high solubility for these redox couples, result in a high ionic conductivity of these redox couples, and are flexible.[14] However, they can also leak and suffer from parasitic heat transport, frustrating the formation of sharp and stable temperature gradients.[20-22] Gelled electrolytes represent an attractive and tuneable middle ground, retaining flexibility and potentially high ionic conductivity while frustrating bulk heat conduction and preventing leakage issues.

To date only one report appears to mention gelled electrolytes in the context of thermocells; Manda *et al.* reported a 'thermocell' using an agar agar gelled electrolyte.[23] However, no comparison was made with non-gelled systems, and only ferricyanide was employed, so balanced redox processes could not have occurred without ferrocyanide present. This likely accounts for why 'Seebeck coefficients' well outside of expected and reasonable values were reported, and which fluctuated randomly *e.g.* 1 M potassium ferricyanide giving Seebeck values of +12.9 mV K^{-1}, -5.2 mV K^{-1} and +4.2 mV K^{-1} at ΔT values of 30, 50 and 70 K, respectively.[23] Brown *et al.* have investigated the Seebeck coefficient and the reversibility of the inherent thermoelectrochemistry present in artificial collagen hydrogels and shark-derived hydrogels, to probe the sensory transduction mechanisms of sharks.[24]

Conversely, gelling electrolytes in secondary acid batteries have been comprehensively demonstrated to extend lifetime, improve discharge cycle reproducibility, lower electrolyte stratification, reduce leakage of the electrolyte, reduce corrosion, increase resistance to thermal runaway events, *etc.*[25, 26] Devices based on gelled electrolytes can also be freely installed and utilised under any orientation, unlike (even extremely viscous) liquid electrolytes.[27]

A gel may be defined as a form of matter intermediate between solid and liquid that shows mechanical rigidity, and forms a viscoelastic system where the 'storage modulus' (G') is larger than the 'loss modulus' (G").[28] The simplest and most common test for this is the 'inversion test'; when a sample in a container is turned upside down, a gel will not flow under its own weight (as it possesses a higher G' than G"), while even a viscous liquid will show significant flow.[29]

The formation, structure and characteristics of gels differ depending on the gelling agent used, but generally follows the basis of 'junction zones'.[30] Here distinct phases of gelling agent are present with a solvent in the interstices, to form a three-dimensional heterogeneous network. Such associations in aqueous systems are frequently driven by hydrogen bonding, hydrophobic associations and electrostatic interactions.[28]

A significant gelling agent for aqueous solutions is agar agar. It is mainly composed of the polysaccharide agarose, a linear polysaccharide consisting of 1, 3-linked β-D-galactopyranose and 1, 4-linked 3, 4-anhydro-α-L-galactopyranose.[31] When dissolved and precipitated from water (*i.e.* by heating and cooling), a three-dimensional network of cross-linked polymers self-assembles via hydrogen bonding and hydrophobic interactions, which hold the electrolyte solution in place.[28] Silica nanoparticles (in the form of fumed silica) are also widely employed to gel acidic aqueous electrolytes.[25, 26]

Other polymers are also known to 'immobilise' water, such as zwitterionic or polyionic polymers. For example, poly(acrylic acid) can be cross-linked to form 3D beads (typically via inverse polymerisation methods), converted to the sodium salt, and dried. This results in a free-flowing super-adsorbent powder composed of poly(sodium acrylate) which, when exposed to water, can easily expand within seconds to at least one order of magnitude higher volume and two orders of magnitude higher mass.[32]

In this investigation, we have rigorously compared the thermoelectrochemical properties of aqueous ferri/ferrocyanide solutions, both gelled and un-gelled. Conventional agar agar-based gels and novel poly(sodium acrylate)-based gels selected for in-depth exploration. The interaction of the ferri/ferrocyanide and the electrolyte with the stainless steel CR2032 battery casings used to house the samples necessitated surface chemistry and long-term discharge studies. Heat transport through the cells was also monitored, and modelling employed to explain the observed results. Ultimately, the gelled electrolytes were able to demonstrate improved long-term stability, and beneficially frustrated heat transport, and thus show their significant potential in the context of thermocells.

2. Experimental

2.1 Instrumentation

All cyclic voltammograms were recorded using a μAutolab PGSTAT 101 via Nova software (EcoChemie, Utrecht, The Netherlands), and a Micrux thin film platinum electrode (diameter 1 mm, ED-SE1-Pt, Micrux, Oviedo, Spain). The Micrux electrodes were 'pre-conditioned' in between each experiment by repeatedly scanning between +0.5 V and -0.5 V in aqueous 0.1 M $K_3[Fe(CN)_6]$ / 0.1 M $K_4[Fe(CN)_6]$; no other form of cleaning or activation was performed. All other measurements were performed inside CR2032 battery casings (MTI Corporation, Richmond, CA, USA). These can contain *ca.* 0.7 mL electrolyte, and were hermetically sealed using an MSK-110 hydraulic crimping machine (MTI Corporation) before use. Platinum-coated CR2032 casings were supplied by MTI Corporation.

Thermoelectrochemical measurements were made using an in-house constructed temperature-control apparatus which has been described in detail elsewhere;[14, 19] a schematic of the overall layout is displayed in Figure S1 in the Supplementary Data. All cells were measured in a thermally 'parallel' arrangement, as shown in Figure S1. This arrangement is distinct from hot-over-cold or cold-over-hot electrode arrangements, which can have significantly suppressed or enhanced convection, respectively.[33] Thermoelectrochemical measurements were recorded using a Keysight B2900A Source Measure Unit (TRIO Test & Measurement Pty Ltd, Australia). The open circuit potential and current values determined by measuring continuously for 10 min, and averaging the final 5 min data, unless otherwise specified. Current was converted to current density using the exposed surface area inside the CR2032 casing.

2.2 Reagents

Potassium ferricyanide(III) $K_3[Fe(CN)_6]$, potassium ferrocyanide(II) trihydrate $K_4[Fe(CN)_6]\cdot 3H_2O$ and fumed silica powder (0.007 μm) were obtained from Sigma-Aldrich (Castle Hill, Australia). Food-grade agar agar powder and gelatine powder were obtained from a local supermarket. The anhydrous poly(sodium acrylate) powder was obtained as an 'Expanding Snow Lab Pack' (Prof Bunsen's Science, Point Cook, Australia). All solutions were prepared with MilliQ^{TM} water (resistivity ≥ 18.2 MΩ cm^{-1}), and all reagents used as received.

2.3 CR2032 casing pre-treatment

The CR2032 coin cell battery casings were either; used as received; soaked in a large excess of absolute ethanol for *ca.* 24 h; soaked in a large excess of 0.1 M $K_3[Fe(CN)_6]$ / 0.1 M $K_4[Fe(CN)_6]$ electrolyte for specified durations; or immersed in 1 M H_2SO_4 for exactly 10 s. All casings were subsequently rinsed thoroughly with water and dried with a KimWipe tissue.

2.4 Gel preparation

All agar agar and gelatine gels were made by combining water or the liquid electrolyte with the specified wt% of powder and then simmered for 20 min in a covered beaker before being placed in a fridge at 4°C to set. Weight measurements before and after were used to ensure evaporative loss did not exceed more than 1% of the total mass.

All fumed silica and poly(sodium acrylate) gels were prepared by combining the required amount of solid and liquid, briefly agitating at room temperature, and then sonicating for 10 min before being stored at room temperature.

2.5 Thermal conductivity measurements

Thermal conductivity was measured using a KD2 Pro Thermal Properties Analyzer and a 1.3 mm by 60 mm needle sensor (Decagon Devices Inc., US). The aqueous and gelled electrolytes were prepared in 50 mL poly(propylene) centrifuge tubes, which were thermally equilibrated in an air-conditioned laboratory prior to measurement (T = 22 ± 0.5°C, as recorded by the KD2 Analyzer). The needle was inserted vertically into the sample to minimise free convection, and at least a 15 minute wait time was applied between each measurement (repeated 3 to 9 times).

3. Results & Discussion

3.1 Preparation of gels and gelled electrolytes

Initial tests involved forming gels with water and comparing the process with an aqueous ferri/ferrocyanide electrolyte. Burrows investigated the thermoelectrochemical properties of up to 0.2 M potassium ferricyanide ($K_3[Fe(CN)_6]$) and 0.2 M potassium ferrocyanide ($K_4[Fe(CN)_6]$);[7]; later Mua and Quickenden optimised the electrolyte as 0.26 M $K_3[Fe(CN)_6]$, 0.26 M $K_4[Fe(CN)_6]$ and 0.8 M potassium chloride (KCl).[2, 34] Since then *ca.* 0.2 to 0.26 M each of $K_3[Fe(CN)_6]$ and $K_4[Fe(CN)_6]$ have been routinely employed.[11, 13, 21, 34-42] However, the solution of Mua and Quickenden was found to be not fully soluble below temperatures of *ca.* 25°C (evident by KCl crystals). Additionally, 0.26 M $K_3[Fe(CN)_6]$ and 0.26 M $K_4[Fe(CN)_6]$ in the absence of KCl was found to be supersaturated at the lowest temperatures employed here (10°C), resulting in precipitation upon the cooler electrode (evident by $K_4[Fe(CN)_6]$ crystals). Therefore 0.1 M of each, henceforth referred to as 0.1 M $K_3[Fe(CN)_6]$ / 0.1 M $K_4[Fe(CN)_6]$, was used as no precipitation was evident upon extended storage at 4°C.

Gelling was investigated using a polysaccharide (food-grade agar agar), a protein (food-grade gelatine powder), a nanomaterial (fumed silica), and a novel approach to gelling was also

investigated using small beads of poly(sodium acrylate) (sold as 'magic snow' for chemistry outreach events). Each prospective gelling agent was mixed at five different ratios (1 wt% to 10 wt%) with both ultrapure water and the 0.1 M $K_3[Fe(CN)_6]$ / 0.1 M $K_4[Fe(CN)_6]$ electrolyte; agar agar and gelatine systems were heated to their boiling point before being left at 4°C to set, while the poly(sodium acrylate) beads and fumed silica were mixed with the liquids using first manual stirring then ultrasonication for 10 min. Gelation was determined using the well-known 'inversion' test;[29] Table 1 summarises the ratios found to form good gels.

		1 wt%	**2 wt%**	**3.3 wt%**	**6.6 wt%**	**10 wt%**
Agar Agar	Water	Gel	Gel	Gel	Gel	Gel
	Electrolyte	**X**	**Gel**	**Gel**	**Gel**	**Gel**
Gelatine	Water	X	Gel	Gel	Gel	Gel
	Electrolyte	**X**	**X**	**X**	**Gel**	**Gel**
Poly(sodium acrylate) beads	Water	Partial	Partial	Gel	Gel	Gel
	Electrolyte	**X**	**X**	**X**	**Gel**	**Gel**
Fumed Silica	Water	X	X	X	Partial	Partial
	Electrolyte	**X**	**X**	**X**	**X**	**X**

Table 1: *Reporting the effectiveness of the different gelling agents for water and the electrolyte 0.1 M $K_3[Fe(CN)_6]$ / 0.1 M $K_4[Fe(CN)_6]$; 'gel' indicates it passed the inversion test, 'partial' indicates only part of the material passed the inversion test, and 'X' indicates all material failed the inversion test*

All systems were found to be more effective at gelling pure water than the electrolyte, due to electrostatic screening in the latter system. Both agar agar and poly(sodium acrylate) beads were

found to be effective gelators for the electrolyte, so were selected for further study. The electrolyte-containing gelatine gels were found to melt at relatively low temperatures (~35°C) so were not investigated further. Fumed silica is widely utilised for gelling strongly acidic aqueous electrolytes,[25, 26] but was unable to form effective gels with the employed neutral solutions.

Further optimisation of gels formed with poly(sodium acrylate) beads demonstrated that 5.5 wt% was the lowest possible gelator content and also resulted in the most homogeneous and transparent gels. For this reason, all further investigation utilised either 5.5 wt% poly(sodium acrylate) beads or agar agar in the 0.1 M $K_3[Fe(CN)_6]$ / 0.1 M $K_4[Fe(CN)_6]$ electrolyte. Figure 1(a) displays a photograph of the 5.5 wt% poly(sodium acrylate) gels formed with just water (transparent) and with 0.1 M $K_3[Fe(CN)_6]$ / 0.1 M $K_4[Fe(CN)_6]$ (yellow). The individual beads composing the gel can clearly be observed at the gel-air interface; if cut the gel separated into two textured surfaces but reformed on contact, making it a self-healing gel. Figure 1(b) displays a photograph of free-standing 5.5 wt% agar agar gel containing 0.1 M $K_3[Fe(CN)_6]$ / 0.1 M $K_4[Fe(CN)_6]$. As expected for an agar gel, the gel displayed good strength but no inherent self-healing ability.

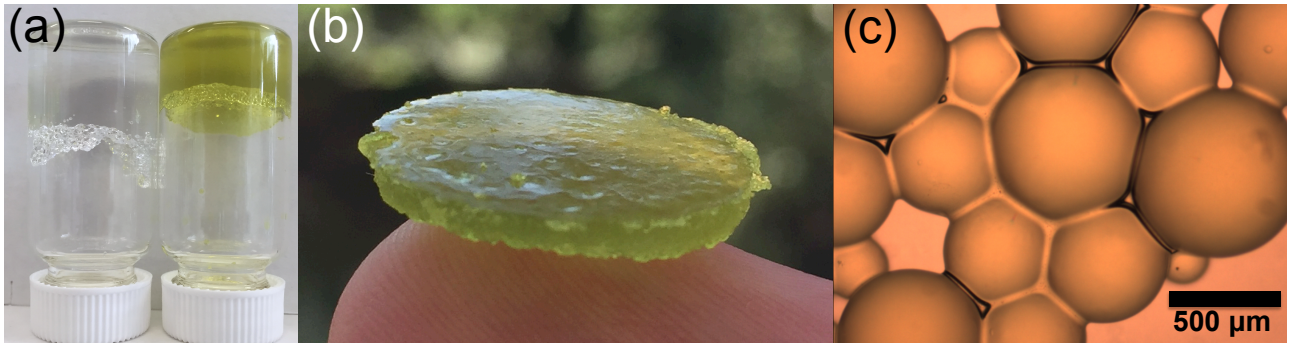

Figure 1: *Displaying photographs of (a) gels prepared with 5.5 wt% poly(sodium acrylate) with just water (transparent) and with 0.1 M* $K_3[Fe(CN)_6]$ */* 0.1 M $K_4[Fe(CN)_6]$ *(yellow), passing the inversion test, and (b) freestanding gel on a fingertip prepared with 5.5 wt% agar agar and 0.1 M* $K_3[Fe(CN)_6]$ */* 0.1 M $K_4[Fe(CN)_6]$*, cut to size for the CR2032 internal cavity. Also shown is (c) an optical microscope image of a thin layer of a typical 5.5 wt% poly(sodium acrylate) gel.*

Microscope evaluation of thin layers of the poly(sodium acrylate) gel clearly highlighted that it was composed of distinct polymeric beads with channels of fluid in-between the beads (Figure 1(c)); small air bubbles or particles were observed to move though these channels by capillary action rapidly. Both solution and polymer phases were equally coloured, implying the equal distribution of $[Fe(CN)_6]^{3-}$ and $[Fe(CN)_6]^{4-}$ between the two phases. These individual polymer-rich beads appear to be gelled together by capillary and Van der Waals forces; some limited hydrogen bonding interactions between carboxylate and carboxylic acid groups are also possible. If compressed, the entire material became featureless, homogeneous and transparent, as can be observed in the bulk of the gel in the photograph in Figure 1(a). Conversely, the agar agar gel was featureless during evaluation by microscope; the structure of agar agar gels are dominated by interactions and chains on the nanometer scale.[43] The polysaccharide chains in agar gel are known to superaggregate (chains form double helices which further aggregate in groups of 10 to 10,000 to form filaments which join end to end), resulting in pores, which form channels through the gel.[43] The pores in the agar agar gel are expected to be *ca.* 50 nm in diameter at the employed agar agar content.[44]

3.2 Cyclic Voltammetric characterisation of the electrolytes

The electrochemistry of the 0.1 M $K_3[Fe(CN)_6]$ / 0.1 M $K_4[Fe(CN)_6]$ electrolyte was evaluated, firstly just dissolved in water, and later after the same solution had been gelled with 5.5 wt% poly(sodium acrylate) or agar agar. No other supporting electrolyte was added, and electrochemistry was performed using a Micrux thin film single electrode where three platinum (Pt) electrodes have been printed onto glass. Consequently, the drop of aqueous electrolyte could be placed on top, or the glass slide could be forced into a section of gel, and identical cell geometry maintained.

Figure 2(a) displays a cyclic voltammogram (CV) for the aqueous 0.1 M $K_3[Fe(CN)_6]$ / 0.1 M $K_4[Fe(CN)_6]$ redox couple (—), which displays the anticipated reversible redox chemistry. The

poly(sodium acrylate) beads were explicitly chosen as they are strongly polyanionic in water, indicating they should not electrostatically retain the tri- or tetra-anionic $[Fe(CN)_6]^{3-}$ and $[Fe(CN)_6]^{4-}$ redox species. Promisingly, voltammetry in the poly(sodium acrylate) gel (---) was almost identical to that observed in the aqueous electrolyte. Conversely, the current density for the agar agar system (—) was *ca.* 50% of that observed in the other two systems.

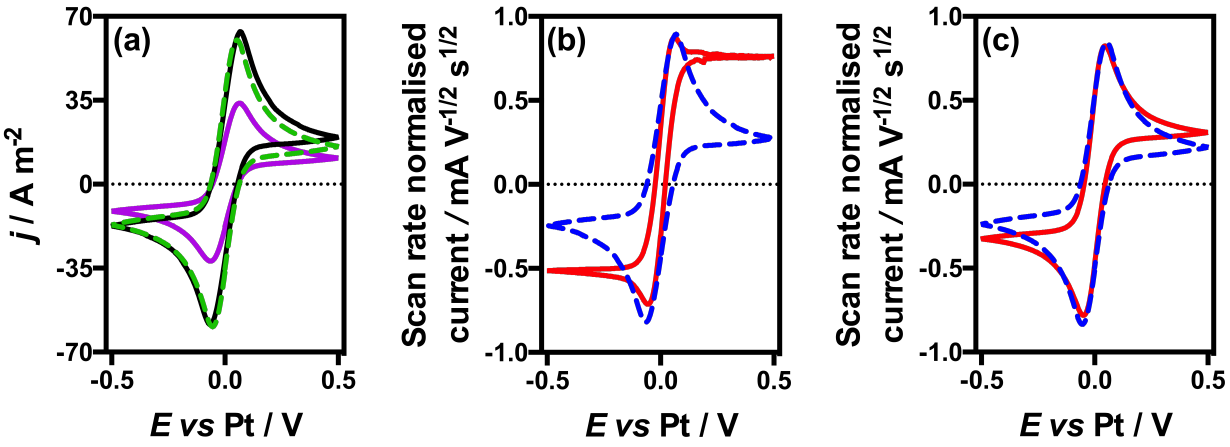

Figure 2: *(a) Cyclic voltammetry for 0.1 M $K_3[Fe(CN)_6]$ /* 0.1 M *$K_4[Fe(CN)_6]$ as a liquid aqueous electrolyte (—), 5.5 wt% poly(sodium acrylate) gel (---) and 5.5 wt% agar agar gel (—) at* ca. *20°C and 50 mV s^{-1}. Also shown are scan-rate normalised cyclic voltammograms at 50 mV s^{-1} and 5 mV s^{-1} for (b) liquid and (c) 5.5 wt% poly(sodium acrylate) gelled 0.1 M $K_3[Fe(CN)_6]$ /* 0.1 M *$K_4[Fe(CN)_6]$.*

The significant reduction in the current density upon moving from the aqueous electrolyte to the agar agar gelled electrolyte (by *ca.* a factor of 2) is consistent with prior observations. For example, the apparent diffusion coefficient of $[Fe(CN)_6]^{3-}$ has been noted by decrease by a factor of 1.2 (in 2 wt% agarose gel),[45] 1.4 (in 3% agar gel)[46] and 2.6 (in 1% agarose gel,[47] relative to a similar ungelled aqueous electrolyte; this change is sensitive to the quantity of gelling agent,[48]

concentration of redox probe[48] and potentially even the time duration of the diffusion measurement itself.[49] Even greater differences have been observed for $[Fe(CN)_6]^{4-}$, such as a factor of 4.8 in 3% agar gel.[50, 51]

Gelled electrolytes have been demonstrated to allow 'container-less' voltammetry, with the voltammetric response remaining ideal (*i.e.* convection-free) even at extremely slow scan rates.[47] Scan rate studies on our systems demonstrated significant deviation at slower scan rates in the liquid electrolyte, as demonstrated by the normalised scans in Figure 2(b); this deviation can be attributed to both bulk thermal convection and potentially electromigration, with the latter since no other supporting electrolyte was added. The poly(sodium acrylate) gel (Figure 2(c)) retained voltammetry closer to ideal responses, down to much slower scan rates, as expected for gelled electrolytes. Voltammetry in the agar agar gel (shown in Figure S2 in the Supplementary Data across a wide range of scan rates) also displayed minimal deviation across scan rates, due to nearly complete suppression of bulk convection.

While Figure 2(a) demonstrates maximum possible current densities, relating the voltammetry to physicochemical differences in the systems is challenging. For example, no supporting electrolyte has been added. Therefore electromigration will be significant in the aqueous electrolyte, but less so in the polyionic poly(sodium acrylate) gel. The molality of the redox compounds was decreased by the addition of 5.5 wt% poly(sodium acrylate) or agar agar (from 0.1 mol kg^{-1} to 0.095 mol kg^{-1}), but the precise concentrations (in mol L^{-1}) are unknown; the poly(sodium acrylate) gel is also heterogeneous, and the concentration inside and outside of the beads are not necessarily identical. However, assuming the concentration is largely unchanged, the free-flowing micron-sized channels of electrolyte present in the poly(sodium acrylate) gel must be responsible for the aqueous-like current densities over short time scales (*cf.* Figure 2(a)) while the system still acts like a bulk gel on longer time scales and length scales (*cf.* Figure 2(c)).

3.3 Initial thermoelectrochemical evaluation of aqueous potassium ferri/ferrocyanide at stainless steel electrodes in CR2032 battery casings

The Seebeck coefficient of aqueous $[Fe(CN)_6]^{3-}$ / $[Fe(CN)_6]^{4-}$ has been reported to be between -1.0 and -1.72 mV K^{-1},[1, 2] with the Seebeck coefficient generally increasing for simple systems as the concentration decreases, in line with Debye–Hückel theory.[14] Salazar *et al.* have reported the Seebeck coefficient of 0.1 M $K_3[Fe(CN)_6]$ / 0.1 M $K_4[Fe(CN)_6]$ as *ca.* -1.5 mV K^{-1}.[40]

For power measurements, a hermetically sealed system with relatively large electrode surface areas and small electrode-to-electrode separation are ideal; CR2032 coin cell battery casings have been previously reported for this reason.[11, 14, 19, 35, 52] Hence a CR2032 casing was used to house the electrolytes for direct comparison, although it should be noted that the gels did not specifically require this.

A temperature regime appropriate for harvesting radiative body heat was investigated. Since the surface of the human skin can be reasonably expected to be between 31 and 38°C (depending upon anatomic location and the surrounding thermal environment),[53] the 'hot' electrode of the CR2032 cell was fixed at 35°C. The 'cold' electrode was varied between 10°C and 30°C; the absolute average world surface temperature is currently *ca.* 14°C.[54] The cell potential and power were evaluated by gradually increasing the temperature of the cooler electrode from 10°C to 30°C in 5°C increments, representing ΔT values between 25°C and 5°C, respectively. Figure 3(a) displays an example of the recorded thermoelectrochemical data, with the cell potential at ΔT = 25°C recorded for 1,000 s, and then the cold electrode temperature was increased by 5°C each further 1,000 s. The cell potential correspondingly decreased as ΔT decreased.

Figure 3(b) plots the cell potential from Figure 3(a) as a function of ΔT, highlighting that the CR2032 battery casing set-up gave an apparent Seebeck coefficient of -1.09 ± 0.04 mV K^{-1}. This is *ca.* 27% lower than the expected Seebeck coefficient of *ca.* -1.5 mV K^{-1},[40] and is consistent with thermoelectrochemical potentials measured in CR2032 casings being lower than those measured by

more impractical but precisely thermostated assemblies.[11, 19, 35, 52] The reason for this is discussed in detail in the modelling section.

Figure 3(c) displays selected power discharge curves for the 0.1 M $K_3[Fe(CN)_6]$ / 0.1 M $K_4[Fe(CN)_6]$ cell at ΔT = 25°C, 15°C and 5°C. As demonstrated by the current output (displayed as dashed lines), the thermoelectrochemical cell acts as a relatively simple V = IR system to yield linear V *vs* I relationships, where the observed resistance is primarily the charge transfer, transport and ohmic resistances.[13] For the power output (P), this is equivalent to P = IV so the power output displays the expected parabola relationship with the maximum power output at cell potential outputs equal to half of the open circuit potential (0.5 V_{OC}) and current outputs equal to half of the short circuit current density (0.5 j_{sc}).

As the ΔT value decreases (by increasing the temperature of the cooler electrode), the thermodynamic driving force (ΔE) is expected to decrease in a linear manner as described by the Seebeck coefficient. This ΔT *vs* ΔE effect in the power output is clearly observed in Figure 3(c); the current density also decreases such that the overall maximum power output decreases by a factor of *ca.* 30 as ΔT decreases from 25°C to 5°C. These results clearly highlight the necessity of maintaining a well-defined temperature gradient across the thermoelectrochemical cell, *e.g.* by ensuring a low thermal conductivity across the system.

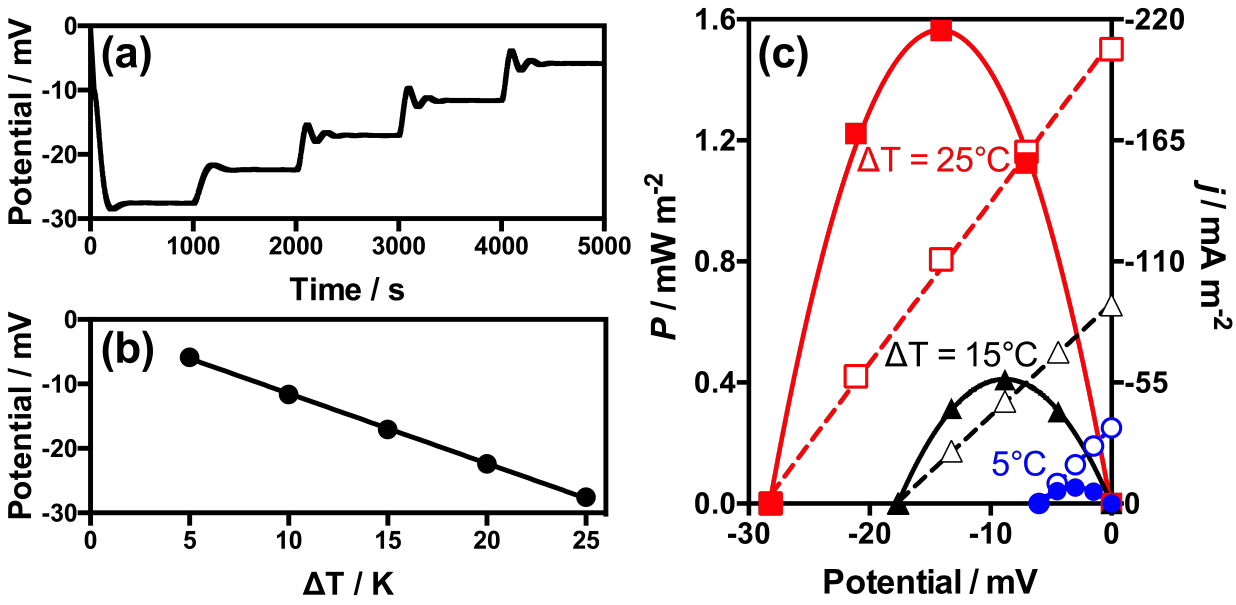

Figure 3 ***(a)*** *Potential of the thermocell when held at T_{hot} = 35°C and T_{cold} = 10°C (ΔT = 25°C) for the first 1,000 s, then T_{cold} increased by +5°C each further 1,000 s, and* ***(b)*** *the resulting linear relationship between potential and ΔT, to give an apparent Seebeck coefficient of -1.09 ± 0.04 mV K^{-1}. Also shown is* ***(c)*** *the power output of the thermocell when T_{hot} = 35°C, and T_{cold} is varied to give ΔT = 25°C (■), 15°C triangles (▲) and 5°C (●). Hollow symbols display current density and filled symbols the overall power output.*

Similar power curves were also obtained for thermocells containing the poly(sodium acrylate) and agar agar gelled electrolytes (Figures S7 and S9, respectively); both displayed the expected parabola power curve. Notably, the current output was relatively stable but not entirely constant for all the cells during the 10 min discharge periods used for each data point in the power curve (*cf.* Figures S8 and S10). The actual stability during extended (hours- and days-long) discharges is discussed later.

Regarding the thermostability of these systems, no issues were encountered in the hermetically sealed casings. With increasing temperature, both gels displayed a greater tendency to flow, although water evaporation (*e.g.* drying out) was a more significant implication of elevated

temperatures. This likely limits them to ambient temperature applications; gelled ionic liquid electrolytes would be required for enhanced stability at elevated temperatures.[19] All subsequent measurements were performed with T_{hot} = 35°C and T_{cold} = 15°C.

3.3 The effect of the stainless steel electrode surface treatment and immersion time upon the thermoelectrochemistry of aqueous potassium ferri/ferrocyanide

The electrochemistry of ferri/ferrocyanide is known to be a quasi-ideal outer sphere redox couple.[16, 55] While it undeniably undergoes outer sphere electron transfer in solution, its rate of electron transfer on the surface of the electrode is influenced by adsorbates, and directly correlates with the presence of 'electrocatalytic' oxygen functionalities.[16, 55] The CR2032 battery casings are mass-produced from 304 stainless steel, and there can be some limited differences between the surface chemistry of the various cells; therefore their reproducibility was investigated.

Battery casings were taken as received, filled with the 0.1 M $K_3[Fe(CN)_6]$ / 0.1 M $K_4[Fe(CN)_6]$ solution, and the open circuit potential and short circuit current density values determined. When freshly prepared, they gave a consistent V_{OC} of -21 ± 1 mV, while the j_{sc} was relatively inconsistent at -276 ± 44 mA m^{-2} (~16% error). With time, j_{sc} further decreased, and uncertainty increased; for this reason three pre-treatment methods were evaluated; (i) soaking the casings in ethanol for 24 h as a 'degreasing step', (ii) immersion in a large volume of 0.1 M $K_3[Fe(CN)_6]$ / 0.1 M $K_4[Fe(CN)_6]$ for between 18 h to drive electrolyte-steel reactions to completion, and (iii) immersion in 1 M H_2SO_4 for 10 s for surface oxidation.

The resulting j_{sc} values are summarised graphically in Figure 4. The j_{sc} for the as-received casings were intermediate, with relatively large error values. Soaking in ethanol or the 0.1 M $K_3[Fe(CN)_6]$ / 0.1 M $K_4[Fe(CN)_6]$ electrolyte resulted in a reduction in the j_{sc}, but also much more reproducible j_{sc} values. Further soaking in the electrolyte (for up to 18 days) only resulted in minor further decreases, indicating a surface modification rather than passivation. Acid treatment resulted

in a dramatic increase in the j_{sc} values, but also unstable j_{sc} values which dropped rapidly with time. The j_{sc} results were compared with a platinum (Pt)-coated CR2032 battery casing. While the Pt casing gives by far the best j_{sc} results (with Pt as a good electrocatalyst), a 10 s immersion of the stainless steel casings in 1 M H_2SO_4 results in the cell achieving *ca.* 33% of the performance of the Pt-coated casing. This merits further investigation, particularly since the cost of Pt-coated casings ($20 USD per casing) far exceeds that of the as-received casings (*ca.* $2.75 USD per casing).

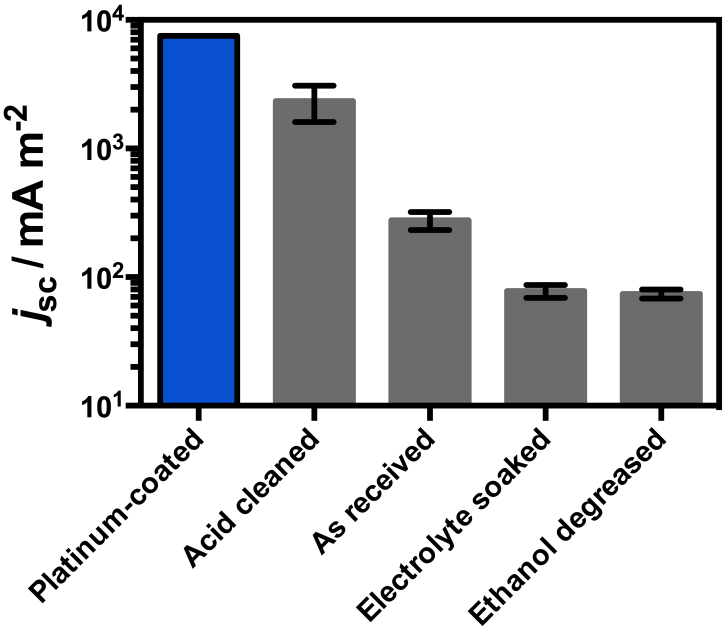

Figure 4: *Plotting the short-circuit current density (j_{sc}) recorded for 0.1 M $K_3[Fe(CN)_6]$ /* 0.1 M *$K_4[Fe(CN)_6]$ at T_{hot} = 35°C and T_{cold} = 15°C, for platinum-coated CR2032 casings (blue) and as a function of the stainless steel CR2032 casing pre-treatment prior to measurement (grey). Error bars represent the 95% confidence interval from measurements on three or more cells.*

These results indicate that oxidising the stainless steel surface results in a significant increase in the current (and therefore power) output; presumably due to an increase in the rate of electron transfer at the oxidised electrode surface. However, this decreased over time, and even as-received cell casings decreased over time upon contact with the electrolyte. Pickling is the removal

of surface oxide on steel, and soluble ferrocyanide salts are known to be potent additives to assist this process,[56] therefore the electrolyte itself is likely responsible for removing the electrocatalytic groups upon the surface. This situation mirrors many oxide-electrocatalytic processes, where optimum electrocatalytic responses are only observed for electrode-electrolyte systems away from their equilibrium.[57]

3.4 Comparison of the three electrolytes during long-term discharge

Having established a thorough understanding of the thermoelectrochemical performance of 0.1 M $K_3[Fe(CN)_6]$ / 0.1 M $K_4[Fe(CN)_6]$ in the stainless steel casing, the two gelled electrolytes and the non-gelled aqueous electrolyte were evaluated by long-term discharge.

Figure 5 displays the short-circuit current density for 0.1 M $K_3[Fe(CN)_6]$ / 0.1 M $K_4[Fe(CN)_6]$ in an as-received CR2032 casing over more than 45 h continuous short-circuiting with T_{hot} = 35°C and T_{cold} = 15°C. The current density was observed to decease gradually overtime. When the same experiment was performed using electrolyte pre-soaked cells (soaked for 24 and 48 h) the current density was lower but also more stable, which is consistent with the observations in Section 3.3; the decrease is therefore due to a gradual drop in the electrocatalytic ability of the stainless steel upon extended exposure to $K_3[Fe(CN)_6]$ and $K_4[Fe(CN)_6]$.

When the poly(sodium acrylate) gelled electrolyte was measured in an as received CR2032 casing, the current initially dropped over the first 60 min of continuous discharge, before stabilising. However, the current was relatively stable even after *ca.* 48 h continuous discharge. This trend in current is somewhat similar to observations by Kang and Hwang when investigating the diffusion of ferrocenemethanol in an agar gel.[49] The diffusion coefficient of ferrocenemethanol is virtually identical in agar-gelled and non-gelled electrolytes [46, 49] and so cyclic voltammetric responses at microelectrodes were similar, but the limiting current during extended coulombic electrolysis at microelectrodes was far lower in the gelled electrolyte due to the lack of natural convection over

longer length scales.[49] In the heterogeneous poly(sodium acrylate) gel, the channels of electrolyte could have sustained higher currents on the minute time scale before diffusion during the gel became more significant during extended discharge.

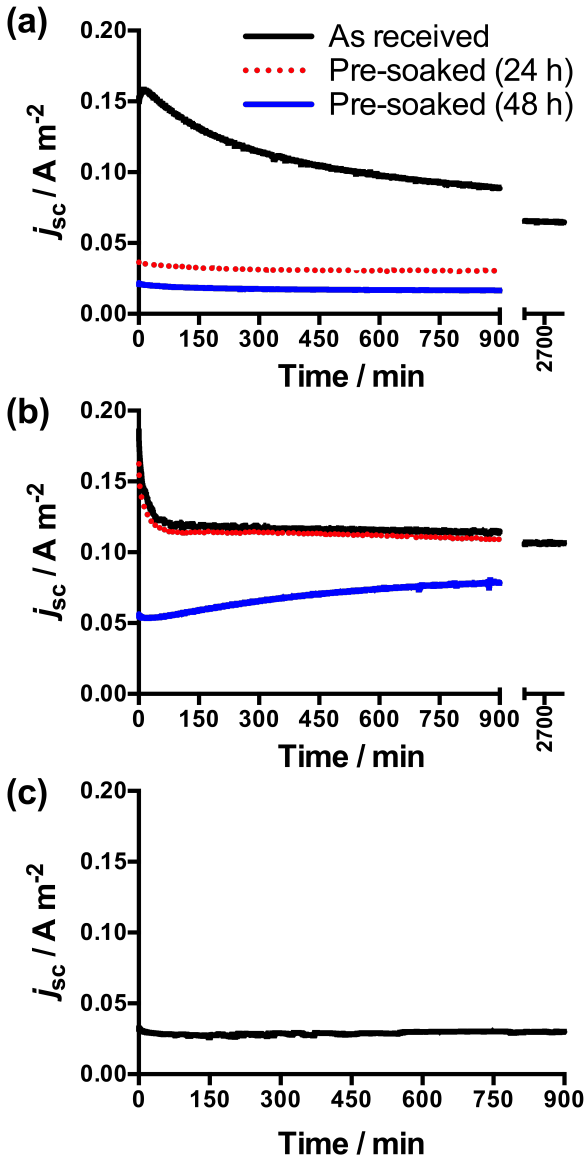

Figure 5: *Plotting the continuous short-circuit current density (j_{sc}) discharge from cells short-circuited for up to 48 h at T_{hot} = 35°C and T_{cold} = 15°C, for (a) ungelled 0.1 M $K_3[Fe(CN)_6]$ /* 0.1 M *$K_4[Fe(CN)_6]$, and the same electrolyte gelled with (b) 5.5 wt% poly(sodium acrylate) and (c) 5.5 wt% agar agar . Cells were either used as received (—), or pre-soaked in a large volume of 0.1 M $K_3[Fe(CN)_6]$ /* 0.1 M *$K_4[Fe(CN)_6]$ for 24 h (---) or 48 h (—) before use. Only 'as received' cells were investigated for agar agar.*

Interestingly, in the poly(sodium acrylate) gel samples the current in casings pre-soaked in the electrolyte for 24 h were essentially indistinguishable from those found in the as-received cell. While the 48 h soaked cell demonstrated a lower initial current density, the current recovered and increased with time. Given this surprising result, the pH of the poly(sodium acrylate) gel was measured and found to be slightly acidic (pH 3.5 for 5.5 wt% poly(sodium acrylate)). This likely stems from the incomplete conversion of the poly(acrylic acid) beads into poly(sodium acrylate). This inherent mild acidity also reveals how the poly(sodium acrylate) gel can maintain an effective electrode surface in the presence of 0.1 M $K_3[Fe(CN)_6]$ / 0.1 M $K_4[Fe(CN)_6]$, and can even reverse extensive prior passivation of the steel, *cf.* the dramatic improvement demonstrated in Figure 4 by just a 10 s pre-treatment with H_2SO_4.

Relatively low current density values were expected for the agar gel, given the lower current in the CV experiments (*cf.* Figure 2). This was found to be the case, with the initial j_{sc} of *ca.* 30 mA m^{-2} far lower than the j_{sc} in the other two systems (Figure 5(c)). Current density also gradually increased with time; while the pH of the fully-formed gel could not be easily investigated, the pH of a viscous solution of water containing 2.25 wt% agar agar was found to be 4.7, again indicating minor beneficial responses when the stainless steel is in contact with these moderately (pH <4.7) acidic gels.

Further experiments were performed to confirm that the lower pH was responsible for improved ferri/ferrocyanide electrochemistry, rather than electrode passivation due to corrosion, or due to boosted thermoelectrochemical performance via thermogalvanic corrosion (*cf.* [11]). Deliberate corrosion of the stainless steel casings with 1 M HCl resulted in obvious tarnishing of the steel surface; the diamond-like indents common to CR2032 casings also rapidly lost their clearly defined shape and became circular. Immersing the casings in 0.1 M $K_3[Fe(CN)_6]$ / 0.1 M $K_4[Fe(CN)_6]$ for *ca.* 9 months did not result in tarnishing, nor other evidence of corrosion. The CR2032 casings containing either liquid 0.1 M $K_3[Fe(CN)_6]$ / 0.1 M $K_4[Fe(CN)_6]$ electrolyte, or the moderately acidic (pH 3.5) 5.5 wt% poly(sodium acrylate)-gelled electrolyte, were also opened

after long-term discharge experiments and housing the electrolyte for *ca.* 9 months; once again, no tarnishing nor loss of the indented shape was observed, in either case (Figure S11), confirming corrosion was not significant in either system.

Finally, casings which had been soaked in 0.1 M $K_3[Fe(CN)_6]$ / 0.1 M $K_4[Fe(CN)_6]$ for *ca.* 9 months had their j_{sc} measured while containing (i) 0.1 M $K_3[Fe(CN)_6]$ / 0.1 M $K_4[Fe(CN)_6]$, which had a natural pH of 7.0, and (ii) the same electrolyte which had been deliberately acidified to pH 3.5 with glacial acetic acid. The j_{sc} in the passivated casings for pH 7.0 constantly remained low, while the acidified electrolyte demonstrated a rapid increase in the j_{sc} (Figure S12), consistent with a rapid reversal of the passivation of the steel casing. This confirms that the pH was the most significant effect upon the (in)stability of the j_{sc} and the overall j_{sc} for $K_3[Fe(CN)_6]$ / $K_4[Fe(CN)_6]$ at the steel electrodes, and acidified liquid electrolytes are apparently even more effective than acidic gelled electrolytes.

3.5 Modelling of heat transfer through the CR2032 casings

The effectiveness of thermoelectrochemical systems relies upon having favourable thermodynamics (high Seebeck coefficient), good conductivity of the redox-active species (demonstrated by the long-term steady state j_{sc} values), and ideally frustrated heat transport through the system.

The temperature control apparatus built in-house for our thermoelectrochemical measurements holds the temperature of an aluminium block at a specific temperature by heating or cooling with an adjacent Peltier device. This has already been described in detail elsewhere[14, 19] Importantly, a steady state current will need to be passed through the Peltier device to maintain temperature equilibrium. As this current is known, a relative measure of the energy required to keep one aluminium block at 35°C and the other 15°C (when thermally short-circuited by having a CR2032 battery casing in between them) can be observed. The Arduino microcontroller that

controls this process was modified in this project to record this current, and thus the heating and the cooling process could be evaluated.

In order to measure the relative energy required to maintain thermal equilibrium, four cells were investigated; a crimped but empty CR2032 casing containing only air, and CR2032 cells containing the aqueous 0.1 M $K_3[Fe(CN)_6]$ / 0.1 M $K_4[Fe(CN)_6]$ electrolyte and the two gelled electrolytes. The current required to maintain the 'hot' aluminium block at 35°C was found to be constant for three of the cells, but *ca.* 7% higher for the cell containing the aqueous 0.1 M $K_3[Fe(CN)_6]$ / 0.1 M $K_4[Fe(CN)_6]$ electrolyte. The current required to maintain the cooler block at 15°C displayed greater variation; the values are displayed graphically in Figure 6. Relative to the current required to maintain thermal equilibrium across the empty casing, the cell containing the agar agar gel required only *ca.* 2% more energy and the cell containing the poly(sodium acrylate) gel required *ca.* 20% more energy. Conversely, the cell containing the aqueous electrolyte required *ca.* 2.4 fold more energy to maintain thermal equilibrium. These results indicate that the aqueous cell is transporting significantly more thermal energy than the other cells.

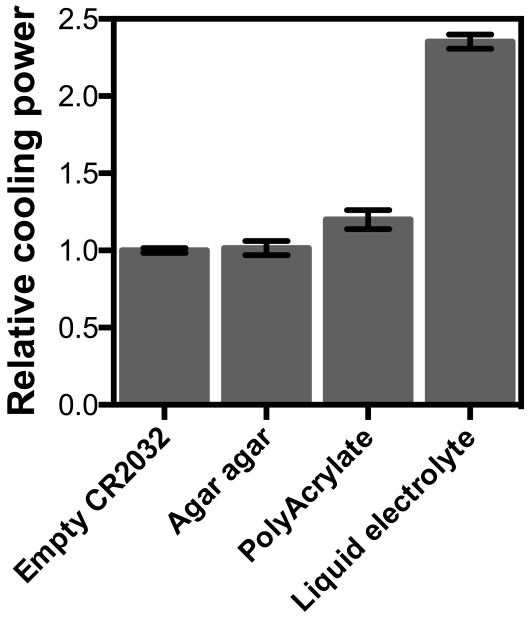

Figure 6: *Relative cooling power required to maintain the cooler aluminium block at 15°C when thermally short-circuited by a CR2032 casing containing the material on the x-axis. Error bars indicate variation in the required cooling power observed over an 18 h period*

In thermocells, passive heat transport can occur through the electrolyte and even the thermocell casings. The additional ion flux occurring between the anode and cathode during thermocell discharge can also conduct additional quantities of thermal energy. However, when the cells were tested in this study under both short-circuit conditions and when unconnected, the difference in the cooling and heating power were within error (*ca.* 2% max). Therefore passive heat transfer is dominant in all of these cells, although this situation would likely alter if the current density were significantly enhanced (*e.g.* through the use of electrocatalysts, nanostructured electrodes or higher concentrations).

To investigate why the liquid-based thermocell was so different from the air- and gel-containing thermocells, and yet the temperature-dependant open circuit potentials were essentially identical, very preliminary modelling of heat transport through the entire system was performed. Figure 7(a) displays the general schematic of the modelled system, while Table S1 in the Supplementary Data summarises the utilised physical parameters. The left-hand side of Figure 6(c) and 7(d) displays colour-coded 'heat maps' for a CR2032 casing containing air and water, respectively. Notably, both the hotter and cooler electrodes directly reflected the temperatures of the hotter and cooler aluminium block (35°C and 15°C, respectively), and maintained constant temperature gradients across the cell. The consistent temperature in the metals is because the thermal conductivity of the aluminium block (*ca.* 204 W m^{-1} K^{-1}) and stainless steel casing (*ca.* 16.2 W m^{-1} K^{-1}) are orders of magnitude more than the thermal conductivity of both air and water (*ca.* 0.0257 and 0.16 W m^{-1} K^{-1}, respectively).

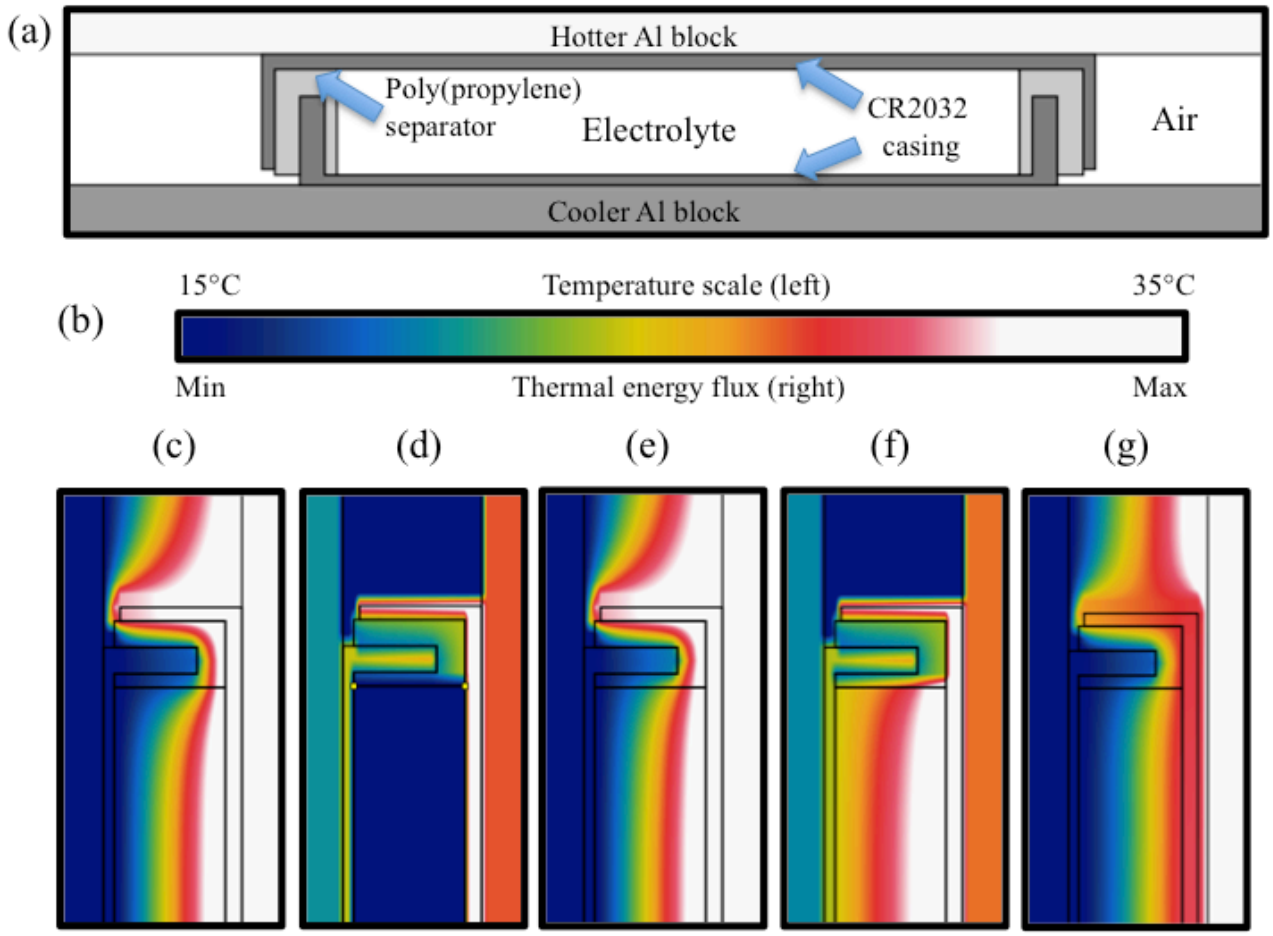

Figure 7: *(a) Schematic of the CR2032 battery arrangement used for modelling (real measurements and modelling were performed rotated 90° right relative to the images, as shown below), with the CR2032 casing 2.0 mm tall and 32.0 mm wide, and (b) the 'rainbow' colour-code for the displayed temperature (heat) maps and thermal energy flux maps. Also shown are; the (c) heat map and (d) thermal energy flux map for a CR2032 casing when filled with air, shown in the orientation that it was modelled in; the (e) heat map and (f) thermal energy flux map for a CR2032 casing when filled with water; and (g) the resulting heat map when a 15 µm air gap is introduced between the hotter aluminium block and a water-filled CR2032 cell, dropping the hot electrode from 35°C to ca. 30°C.*

While the temperature gradients were essentially unchanged by the nature of the electrolyte, variation in the heat flux was much more significant; the right-hand side of Figure 7(c) and 7(d) displays colour-coded 'heat flux maps' for air and water casings, respectively. In the crimped battery casing, an inner layer of poly(propylene) ensures the two metal halves of the cell are electrically insulated from each other and, to a lesser extent, thermally insulated. Although the thermal conductivity of the poly(propylene) is relatively low at *ca.* 0.16 W m^{-1} K^{-1}, it is also relatively thin (from a minimum of *ca.* 0.15 mm to a maximum of *ca.* 0.5 mm). Therefore in the air-containing cell the largest amount of heat flux occurred through the crimped edges of the cell. The reinforced inner steel wall acts as a major heat sink; peak heat flux in this area was *ca.* 150 fold higher than through the air.

In the water-filled cell the *ca*. 2 mm thick layer of water (thermal conductivity *ca.* 0.6 W m^{-1} K^{-1}) can transfer appreciable quantities of heat by itself, and even into the crimped edges through the thin layer of poly(propylene) separating the inner steel layer from the electrolyte. Therefore when filled with water, the cell casing itself transfers an additional *ca.* 38% peak thermal energy relative to air. The peak heat flux through the casing is 10 fold higher than through the water (*cf.* 150 fold when filled air), yet since the water layer has *ca.* 18 fold higher interfacial area, both the casing and water components transport significant quantities of thermal energy.

These two major forms of heat transfer in the water-filled cell account for why the cell containing the aqueous 0.1 M $K_3[Fe(CN)_6]$ / 0.1 M $K_4[Fe(CN)_6]$ electrolyte required the dissipation of *ca.* 2.4 fold more thermal energy to maintain thermal equilibrium in the physical apparatus. Conversely, the cell-casing itself is responsible for virtually all of the heat transfer in the air-filled cell.

The thermal conductivity of the systems was evaluated at ambient temperature (22 ± 0.5°C). The thermal conductivity of aqueous 0.1 M $K_3[Fe(CN)_6]$ / 0.1 M $K_4[Fe(CN)_6]$ (580 ± 20 mW m^{-1} K^{-}

^{1}) was similar to that of water, while the thermal conductivity dropped upon moving to the poly(sodium acrylate) gel (556 ± 1 mW m^{-1} K^{-1}) and agar agar gel (554 ± 2 mW m^{-1} K^{-1}). This 5% decrease in thermal conductivity upon gelation is slightly less that a previously reported 12% reduction upon gelation of water with 5 wt% agar agar.[58] However, factoring this thermal conductivity into the model did not mirror the dramatically reduced heat transfer observed through the real gel-containing cells. Therefore an additional feature is missing from the model; convection. As noted in the cyclic voltammetric section, the gelled electrolytes maintained near-ideal diffusional voltammetric responses over a wide range of temperatures as they suppressed bulk (thermal) convection. Convection was not incorporated into the utilised model (*cf.* rotating our model did not change the outcomes in Figure 7), but is expected to be significant for the liquid system, relatively insignificant for air, and essentially negligible for the gel systems. In particular, Gunawan *et al.* demonstrated significant improvements in power output by altering the orientation of the thermocell to maximise natural convection.[33] Conversely, Hasan *et al.* have recently noted that placing a thin polymeric film in between two electrodes in a weakly thermostated thermocell significantly suppressed thermal convection, as demonstrated by infrared thermal images and improved performance.[59] Therefore, dramatically reduced (convective) transfer of heat is expected in our gelled electrolyte, and the heat transferred via the gel was largely obscured by the thermal energy transferred through the cell housing itself.

Finally, all modelling demonstrated ideal temperature gradients across the two stainless steel electrodes; as such the applied $\Delta T = 20°C$ value was the ΔT value experienced at the electrode-electrolyte interface. Therefore the cells should have consistently demonstrated V_{OC} values of *ca.* 30 mV, whereas values of *ca.* 22 mV were instead consistently observed. This occurred regardless of electrolyte, and is consistent with lower V_{OC} or Seebeck coefficients being observed for every other reported use of CR2032 battery casings as thermocells.[11, 19, 35, 52] Significantly, one side of the CR2032 is actually textured with small bumps, while the other (smoother) side of the CR2032 battery casing developed slight curvature during crimping; both would result in less effective

thermal contact than that predicted by the model. Modelling the system with deliberate air gaps between the heating aluminium block and the CR2032 revealed that even a 15 μm air gap between the two metals was sufficient to drop 5°C across the gap (shown in Figure 7(e)), such that the anticipated V_{OC} value of 30 mV would actually be measured as 22.5 mV. This is because the thermal short-circuit in the CR2032 casing results in a relatively low thermal resistance across the entire thermocell (even when different electrolytes are considered) compared to the thermal resistance of an air-gap. Electrical contact between the two metals was achieved, and therefore a uniform gap of 15 μm was not present across the entire interface between the two metals. However, this highlights that minor contact points between the metals associated with air gaps (>15 μm) across the rest of the interface could be extremely significant.

The observations made during modelling were briefly probed experimentally. The deliberate introduction of thermal paste between the aluminium blocks and the CR2032 casings resulted in less reproducible results, but the V_{OC} was typically higher than those recorded in the absence of the thermal paste. Conversely, placing thin stainless steel metal sheets between the aluminium block and the CR2032 casing resulted in significant drops in the V_{OC} value, despite the thickness of the sheets being negligible. Instead, each additional interface introduced. Theoretically (μm scale) stagnant air layers between the two metal surfaces that possessed relatively significant thermal resistance. Improved interfacial properties are required to overcome these relatively major temperature drops.

One method of assessing the efficiency of such thermo-systems is to divide the maximum power output from the device by the heat flow through the device.[52] Using the thermal conductivity of just the gelled electrolyte, and the power output from these systems in CR2032 casings at ΔT = 20 K and T_{hot} = 308 K (which corresponds to a maximum Carnot efficiency of 6.5%), both liquid- and poly(sodium acrylate)-based cells gave power conversion efficiencies of *ca.* 2×10^{-4} % relative to Carnot efficiency. These low values are not unexpected given the relatively poor electrocatalyst and planar geometry employed; the nanostructuring of electrodes is known to

boost efficiency by orders of magnitude.[52] Regarding the whole device, the overall thermal conductivity is not known so efficiency cannot be calculated. However, given that the relative power output from the poly(sodium acrylate) cells were comparable to or better than that from the liquid-containing cells (*cf.* Figure 5), while the liquid electrolyte-containing cell required twice as much heat dissipation to maintain thermal equilibrium (*cf.* Figure 6). Theoretically, the maximum efficiency of the actual poly(sodium acrylate)-containing thermocells is roughly a factor of two higher than that of the liquid thermocells.

4. Conclusions

In this work we have screened a range of gelling agents for the common thermoelectrochemical electrolyte, aqueous 0.1 M $K_3[Fe(CN)_6]$ / 0.1 M $K_4[Fe(CN)_6]$. A conventional gelling agent, agar agar, and a novel gelling material, poly(sodium acrylate) were found to be appropriate. The agar agar gels were mechanically robust but suffered from low current density values, due to low apparent diffusion coefficients. Conversely, the strongly negatively charged poly(sodium acrylate) was easily formed, and the apparent diffusion coefficients were unchanged (on the voltammetric timescale). Extended testing of thermocells prepared using the gelled electrolyte highlighted improved longevity, likely due to their inherent mild acidity.

The measured open circuit potential values in the CR2032 casings were lower than expected, in agreement with prior literature; modelling and experiments demonstrated this was due to μm-scale air-gaps between the temperature-controlled surfaces and the CR2032 casing. This results in significant (unwanted) thermal gradients between the thermocell and the thermal sink/source, and requires further optimisation. Modelling demonstrated that the CR2032 casing possesses an inherent thermal short-circuit, which is moderately significant when containing aqueous electrolytes but represents the vast majority of (unwanted) heat transfer for gelled electrolytes. Therefore the crimped CR2032 casing is convenient for measurements of

thermoelectrochemical properties but is not recommended as genuine thermocells for harvesting of thermal energy.

5. Acknowledgements

This work was supported by the Australian Research Council (ARC DECRA DE130100770). Prof. R. Atkin and Dr T. Q. To (University of Newcastle, Australia) are thanked for assistance with the thermal conductivity measurements.

6. References

[1] A. Gunawan, C.H. Lin, D.A. Buttry, V. Mujica, R.A. Taylor, R.S. Prasher, P.E. Phelan, Liquid Thermoelectrics: Review of Recent And Limited New Data of Thermogalvanic Cell Experiments, Nanoscale and Microscale Thermophysical Engineering, 17 (2013) 304-323.
[2] T.I. Quickenden, Y. Mua, A Review of Power-Generation in Aqueous Thermogalvanic Cells, J. Electrochem. Soc., 142 (1995) 3985-3994.
[3] J.N. Agar, Thermogalvanic Cells, in: P. Delahay (Ed.) Advances in Electrochemistry and Electrochemical Engineering, Interscience, New York, 1963, pp. 31-120.
[4] A.L. Rockwood, Partial molar entropy of electrons in a jellium model: Implications for thermodynamics of ions in solution and electrons in metals, Electrochim Acta, 112 (2013) 706-711.
[5] J. Newman, Thermoelectric effects in electrochemical systems, Ind. Eng. Chem. Res., 34 (1995) 3208-3216.
[6] J.N. Agar, The rate of attainment of Soret equilibrium, Transactions of the Faraday Society, 56 (1960) 776-787.
[7] B. Burrows, Discharge Behavior of Redox Thermogalvanic Cells, J. Electrochem. Soc., 123 (1976) 154-159.
[8] C.B. Vining, An inconvenient truth about thermoelectrics, Nat. Mater., 8 (2009) 83-85.
[9] K. Shahi, S. Chandra, Emf-Measurements on Thermocell Ag(T1)-Agi-Ag(T2), Zeitschrift Fur Naturforschung Section a-a Journal of Physical Sciences, 30 (1975) 1055-1059.
[10] J.L. Weininger, Thermogalvanic Cells with Silver Iodide as a Solid Electrolyte, J. Electrochem. Soc., 111 (1964) 769-774.
[11] H.A.H. Alzahrani, J.J. Black, D. Goonetilleke, J. Panchompoo, L. Aldous, Combining thermogalvanic corrosion and thermogalvanic redox couples for improved electrochemical waste heat harvesting, Electrochem. Commun., 58 (2015) 76-79.
[12] H. Im, T. Kim, H. Song, J. Choi, J.S. Park, R. Ovalle-Robles, H.D. Yang, K.D. Kihm, R.H. Baughman, H.H. Lee, T.J. Kang, Y.H. Kim, High-efficiency electrochemical thermal energy harvester using carbon nanotube aerogel sheet electrodes, Nature Communications, 7 (2016).
[13] H. Im, H.G. Moon, J.S. Lee, I.Y. Chung, T.J. Kang, Y.H. Kim, Flexible thermocells for utilization of body heat, Nano Research, 7 (2014) 443-452.
[14] J.J. Black, T. Murphy, R. Atkin, A. Dolan, L. Aldous, The thermoelectrochemistry of lithium-glyme solvate ionic liquids: towards waste heat harvesting, Physical Chemistry Chemical Physics, (2016).
[15] M.S. Romano, J.M. Razal, D. Antiohos, G. Wallace, J. Chen, Nano-Carbon Electrodes for Thermal Energy Harvesting, J. Nanosci. Nanotechnol., 15 (2015) 1-14.

[16] F.J. del Campo, P. Godignon, L. Aldous, E. Pausas, M. Sarrion, M. Zabala, R. Prehn, R.G. Compton, Fabrication of PPF Electrodes by a Rapid Thermal Process, J Electrochem Soc, 158 (2011) H63-H68.
[17] T.J. Abraham, D.R. MacFarlane, J.M. Pringle, High Seebeck coefficient redox ionic liquid electrolytes for thermal energy harvesting, Energ Environ Sci, 6 (2013) 2639-2645.
[18] M. Endo, Y. Yamagishi, M. Inagaki, Thermocell with graphite fiber-bromine intercalation compounds, Synth. Met., 7 (1983) 203-209.
[19] E.H.B. Anari, M. Romano, W.X. Teh, J.J. Black, E. Jiang, J. Chen, T.Q. To, J. Panchompoo, L. Aldous, Substituted ferrocenes and iodine as synergistic thermoelectrochemical heat harvesting redox couples in ionic liquids, Chem. Commun. (Cambridge, U. K.), 52 (2016) 745-748.
[20] T. Ikeshoji, F.N.B. Denahui, S. Kimura, M. Yoneya, Computer-Analysis on Natural-Convection in Thin-Layer Thermocells with a Soluble Redox Couple .2. E-I Relation, Electric-Power, Heat-Flux and Electrochemical Heat-Pump, J. Electroanal. Chem., 312 (1991) 43-56.
[21] C.H. Lin, A. Gunawan, P.E. Phelan, D.A. Buttry, V. Mujica, R.A. Taylor, R. Prasher, Optimization of Cell Configuration for Maximizing Performance of a Cu/Cu2+ Aqueous Thermogalvanic Cell, International Mechanical Engineering Congress and Exposition - 2012, Vol 6, Pts a and B, (2013) 541-547.
[22] P.F. Salazar, S. Kumar, B.A. Cola, Design and optimization of thermo-electrochemical cells, J. Appl. Electrochem., 44 (2014) 325-336.
[23] S. Manda, A. Saini, S. Khaleeq, R. Patel, B. Usmani, S. Harinipriya, B. Pratiher, B. Roy, Thermocells of carbon material electrodes and its performance characteristics, Journal of Materials Research and Technology, 2 (2013) 165-181.
[24] B.R. Brown, M.E. Hughes, C. Russo, Thermoelectricity in natural and synthetic hydrogels, Physical Review E, 70 (2004).
[25] D.W.H. Lambert, P.H.J. Greenwood, M.C. Reed, Advances in gelled-electrolyte technology for valve-regulated lead-acid batteries, J Power Sources, 107 (2002) 173-179.
[26] Z. Tang, J.M. Wang, X.X. Mao, H.B. Shao, Q.Q. Chen, Z.H. Xu, J.Q. Zhang, Investigation and application of poly siloxane-based gel electrolyte in valve-regulated lead-acid battery, J Power Sources, 168 (2007) 49-57.
[27] J. Lee, D.S. Silvester, Low-cost microarray thin-film electrodes with ionic liquid gel-polymer electrolytes for miniaturised oxygen sensing, Analyst, 141 (2016) 3705-3713.
[28] D. Saha, S. Bhattacharya, Hydrocolloids as thickening and gelling agents in food: a critical review, J Food Sci Tech Mys, 47 (2010) 587-597.
[29] S.R. Raghavan, B.H. Cipriano, Gel Formation: Phase Diagrams Using Tabletop Rheology and Calorimetry, in: R.G. Weiss, P. Terech (Eds.) Molecular Gels: Materials with Self-Assembled Fibrillar Networks, Springer Netherlands, Dordrecht, 2006, pp. 241-252.
[30] D. Oakenfull, Gelling Agents, Crc Cr Rev Food Sci, 26 (1987) 1-25.
[31] P. Serwer, Agarose gels: Properties and use for electrophoresis, ELECTROPHORESIS, 4 (1983) 375-382.
[32] U. Dayal, S.K. Mehta, M.S. Choudhary, R.C. Jain, Synthesis of acrylic superabsorbents, J Macromol Sci R M C, C39 (1999) 507-525.
[33] A. Gunawan, H. Li, C.-H. Lin, D.A. Buttry, V. Mujica, R.A. Taylor, R.S. Prasher, P.E. Phelan, The amplifying effect of natural convection on power generation of thermogalvanic cells, Int. J. Heat Mass Transfer, 78 (2014) 423-434.
[34] Y. Mua, T.I. Quickenden, Power conversion efficiency, electrode separation, and overpotential in the ferricyanide/ferrocyonide thermogalvanic cell, J. Electrochem. Soc., 143 (1996) 2558-2564.
[35] K.M. Bae, H.D. Yang, L.T. Tufa, T.J. Kang, Thermobattery based on CNT Coated Carbon Textile and Thermoelectric Electrolyte, International Journal of Precision Engineering and Manufacturing, 16 (2015) 1245-1250.
[36] T. Hirai, K. Shindo, T. Ogata, Charge and discharge characteristics of thermochargeable galvanic cells with on [Fe(CN)(6)](4-)/[Fe(CN)(6)](3-) redox couple, J. Electrochem. Soc., 143 (1996) 1305-1313.
[37] T. Ikeshoji, F.N.B. de Nahui, Fundamental analysis on a thermocell with a mixture of the soluble redox couple aqueous potassium ferrocyanide and potassium ferricyanide solution, Journal of Electroanalytical Chemistry and Interfacial Electrochemistry, 296 (1990) 19-36.
[38] T.J. Kang, S.L. Fang, M.E. Kozlov, C.S. Haines, N. Li, Y.H. Kim, Y.S. Chen, R.H. Baughman, Electrical Power From Nanotube and Graphene Electrochemical Thermal Energy Harvesters, Adv. Funct. Mater., 22 (2012) 477-489.
[39] T.I. Quickenden, Y. Mua, The Power Conversion Efficiencies of a Thermogalvanic Cell Operated in 3 Different Orientations, J. Electrochem. Soc., 142 (1995) 3652-3659.

[40] P.F. Salazar, S. Kumar, B.A. Cola, Nitrogen- and Boron-Doped Carbon Nanotube Electrodes in a Thermo-Electrochemical Cell, J. Electrochem. Soc., 159 (2012) B483-B488.
[41] H.D. Yang, L.T. Tufa, K.M. Bae, T.J. Kang, A tubing shaped, flexible thermal energy harvester based on a carbon nanotube sheet electrode, Carbon, 86 (2015) 118-123.
[42] M.S. Romano, N. Li, D. Antiohos, J.M. Razal, A. Nattestad, S. Beirne, S. Fang, Y. Chen, R. Jalili, G.G. Wallace, R. Baughman, J. Chen, Carbon Nanotube – Reduced Graphene Oxide Composites for Thermal Energy Harvesting Applications, Adv. Mater. (Weinheim, Ger.), 25 (2013) 6602-6606.
[43] S. Arnott, A. Fulmer, W.E. Scott, I.C.M. Dea, R. Moorhouse, D.A. Rees, The agarose double helix and its function in agarose gel structure, Journal of Molecular Biology, 90 (1974) 269-284.
[44] J. Narayanan, J.Y. Xiong, X.Y. Liu, Determination of agarose gel pore size: Absorbance measurements vis a vis other techniques, J Phys Conf Ser, 28 (2006) 83-86.
[45] N. Mochizuki, H. Ueno, M. Kaneko, Solid medium for conventional electrochemical measurements, Electrochim Acta, 49 (2004) 4143-4148.
[46] H.L.T. Ho, R.A.W. Dryfe, Transport of Neutral and Ionic Solutes: The Gel/Electrode and Gel/Electrolyte Interfaces, Langmuir, 25 (2009) 12757-12765.
[47] M.H. Lee, Y.T. Kim, Voltammetry in a gel medium, Electrochem Solid St, 2 (1999) 72-74.
[48] H. Ueno, M. Kaneko, Investigation of a nanostructured polysaccharide solid medium for electrochemistry, J Electroanal Chem, 568 (2004) 87-92.
[49] H. Kang, S. Hwang, Electrochemical Characterization of the Hydrophobic Interaction and the Natural Convection within Agarose Gel, Int J Electrochem Sc, 10 (2015) 9706-9713.
[50] K.K. Kasem, Electrochemical behavior of some redox systems pendant in agar gel, J New Mat Electr Sys, 8 (2005) 189-195.
[51] L.S. Books, C. Harris, K.K. Kasem, Electrochemical Behavior of Hexacyano Iron (III/II) in Frozen Aqueous Electrolytes, Am J Undergrad Res, 5 (2007) 25-32.
[52] R.C. Hu, B.A. Cola, N. Haram, J.N. Barisci, S. Lee, S. Stoughton, G. Wallace, C. Too, M. Thomas, A. Gestos, M.E. dela Cruz, J.P. Ferraris, A.A. Zakhidov, R.H. Baughman, Harvesting Waste Thermal Energy Using Carbon-Nanotube-Based Thermo-Electrochemical Cell, Nano Lett., 10 (2010) 838-846.
[53] Y.F. Liu, L.J. Wang, J.P. Liu, Y.H. Di, A study of human skin and surface temperatures in stable and unstable thermal environments, J Therm Biol, 38 (2013) 440-448.
[54] P.D. Jones, M. New, D.E. Parker, S. Martin, I.G. Rigor, Surface air temperature and its changes over the past 150 years, Reviews of Geophysics, 37 (1999) 173-199.
[55] R.L. McCreery, Advanced carbon electrode materials for molecular electrochemistry, Chem Rev, 108 (2008) 2646-2687.
[56] A.E. Chester, J.T. Irwin, Acid pickling of metals and compositions therefor, Poor & Co, 1958.
[57] L. Aldous, R.G. Compton, The mechanism of hydrazine electro-oxidation revealed by platinum microelectrodes: role of residual oxides, Phys Chem Chem Phys, 13 (2011) 5279-5287.
[58] M. Zhang, Z.H. Che, J.H. Chen, H.Z. Zhao, L. Yang, Z.Y. Zhong, J.H. Lu, Experimental Determination of Thermal Conductivity of Water-Agar Gel at Different Concentrations and Temperatures, J Chem Eng Data, 56 (2011) 859-864.
[59] S.W. Hasan, S.M. Said, M.F. Sabri, A.S. Bakar, N.A. Hashim, M.M. Hasnan, J.M. Pringle, D.R. MacFarlane, High Thermal Gradient in Thermo-electrochemical Cells by Insertion of a Poly(Vinylidene Fluoride) Membrane, Sci Rep-Uk, 6 (2016) 29328.